

Investigating exchange efficiencies of sodium and magnesium to access lithium from β -spodumene and Li-stuffed β -quartz (γ -spodumene)

Supplementary information

1. Powder XRD patterns displayed with the full range in 2θ from 5° to 60°

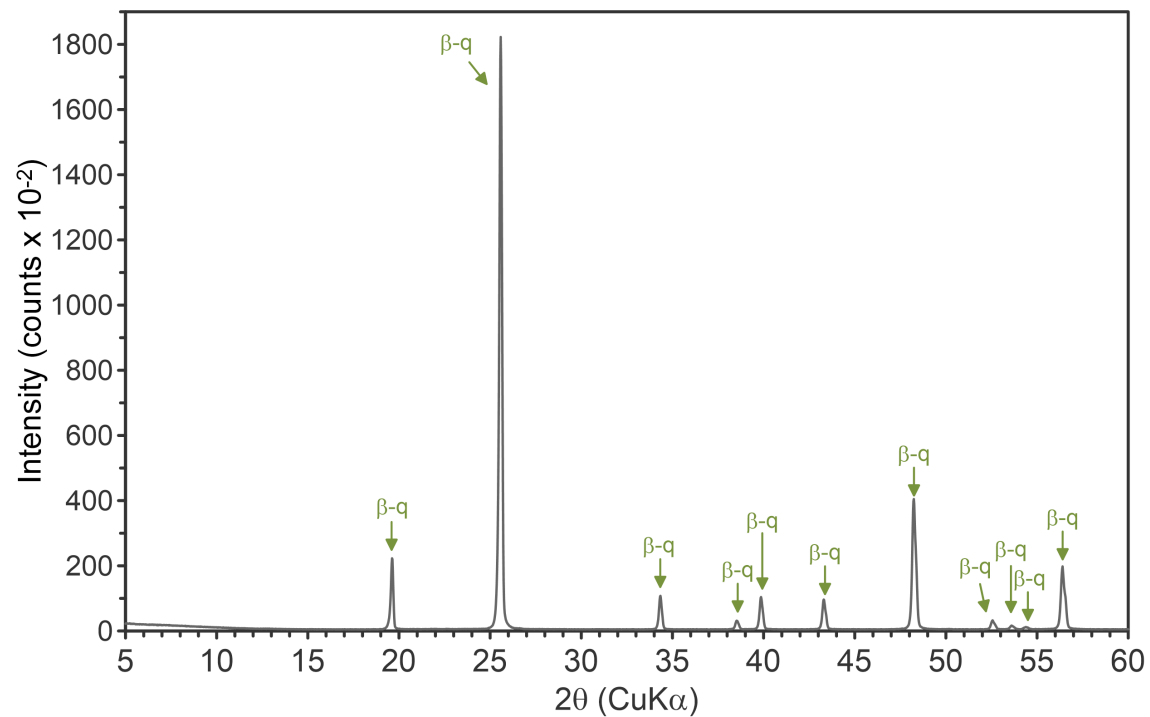


Figure S1. Extended range powder-XRD pattern corresponding to Figure 3a. β -s: β -spodumene; β -q: β -quartz.

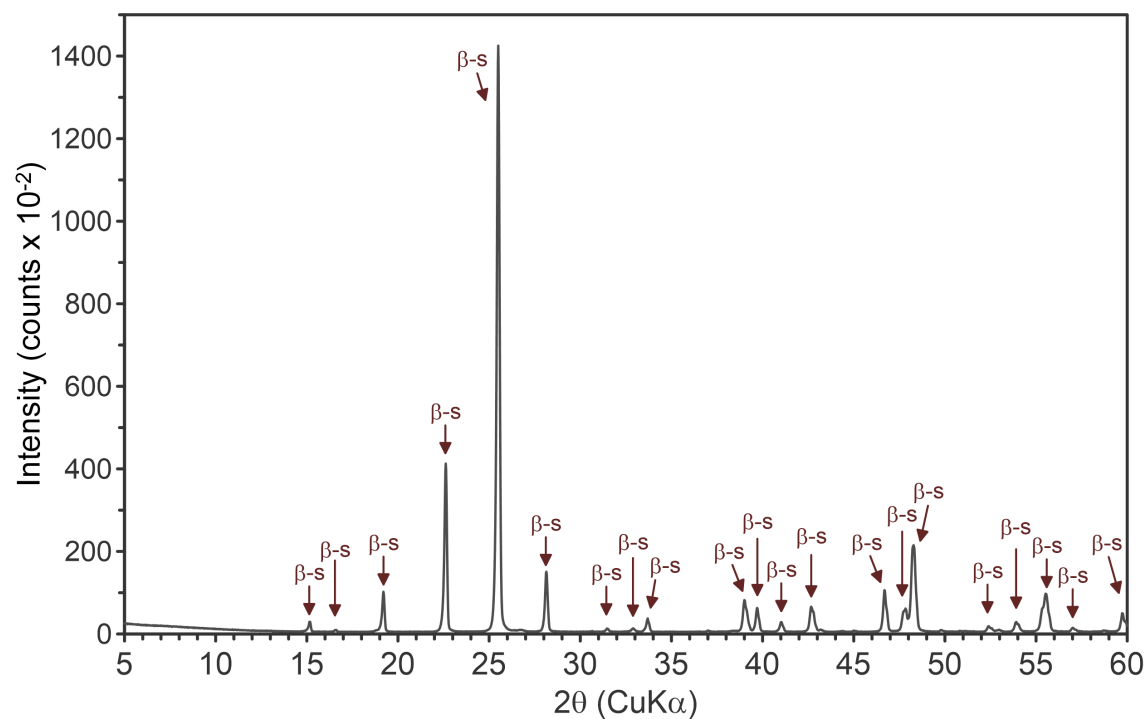


Figure S2. Extended range powder-XRD pattern corresponding to Figure 3c. β-s: β-spodumene; β-q: β-quartz.

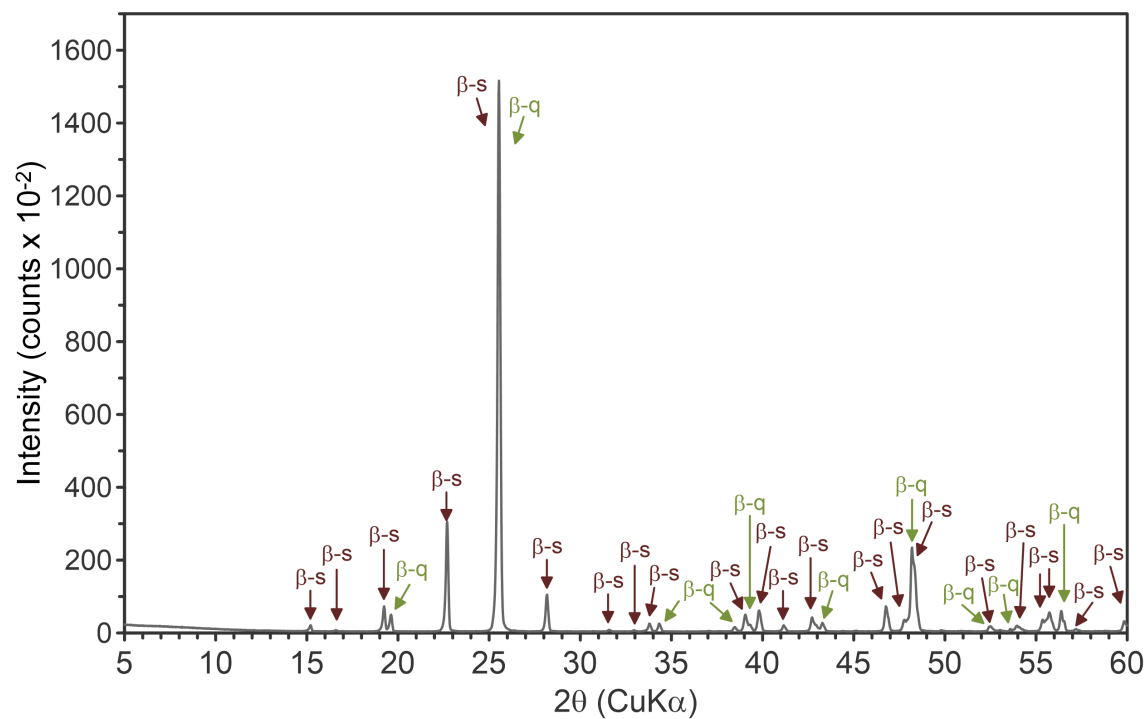


Figure S3. Extended range powder-XRD pattern corresponding to Figure 5a. β-s: β-spodumene; β-q: β-quartz.

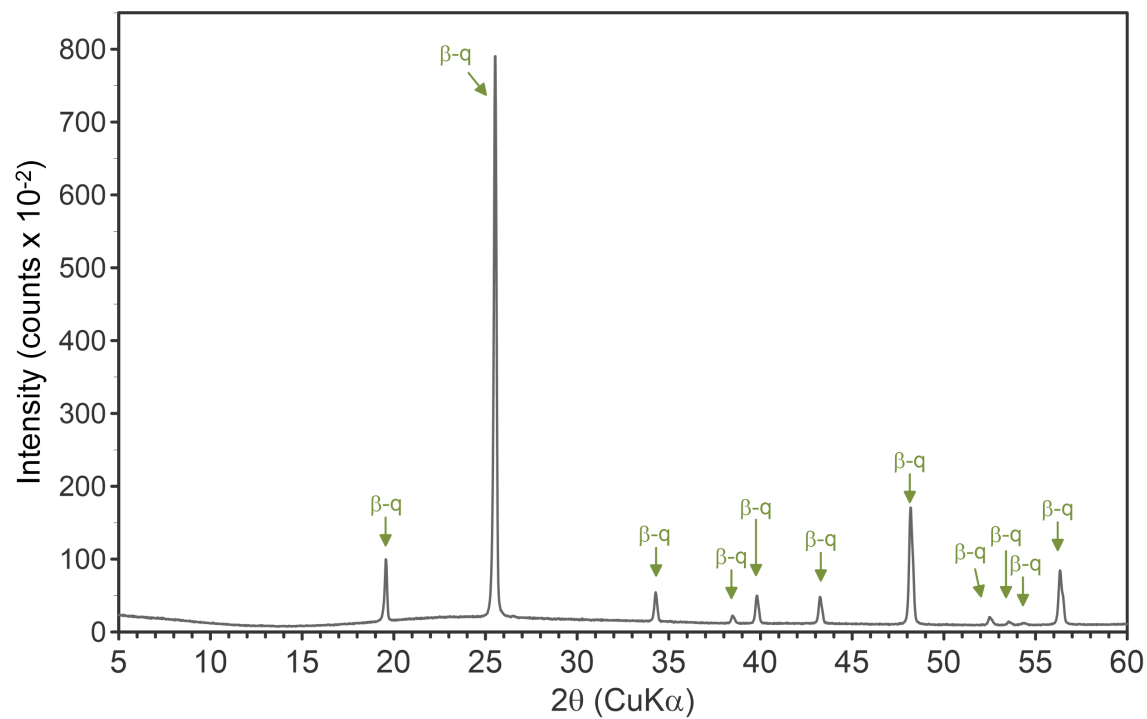


Figure S4. Extended range powder-XRD pattern corresponding to Figure 6a. β -s: β -spodumene; β -q: β -quartz.

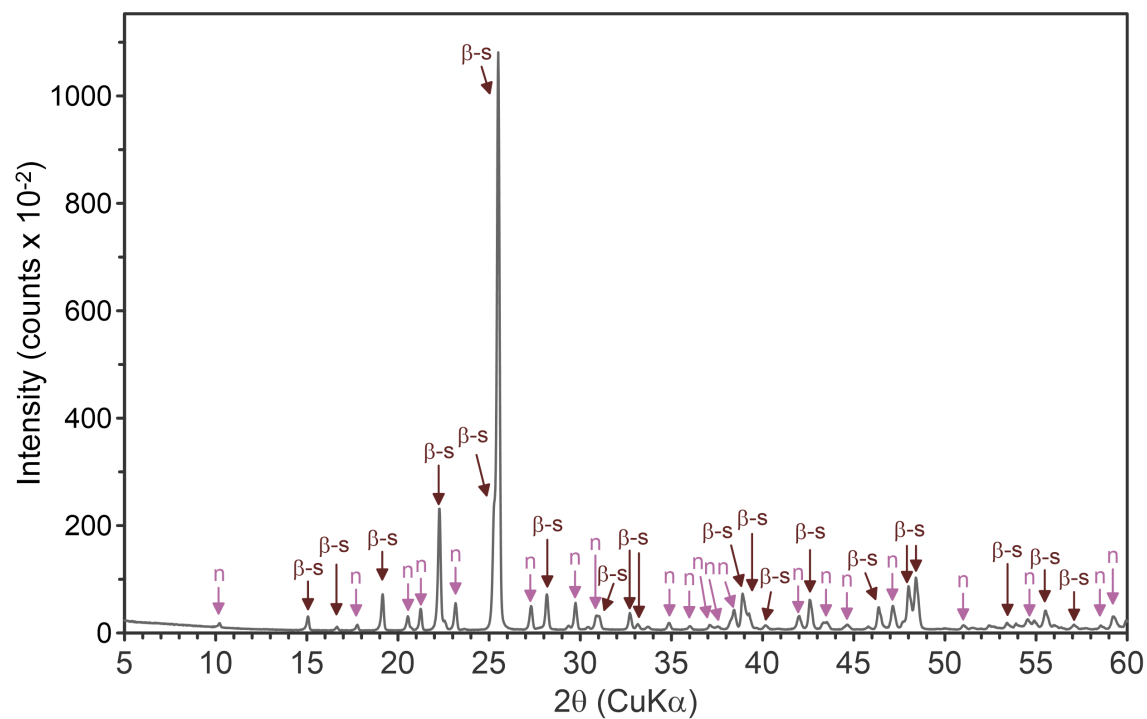


Figure S5. Extended range powder-XRD pattern corresponding to Figure 8a. β -s: β -spodumene; β -q: β -quartz; n: nepheline.

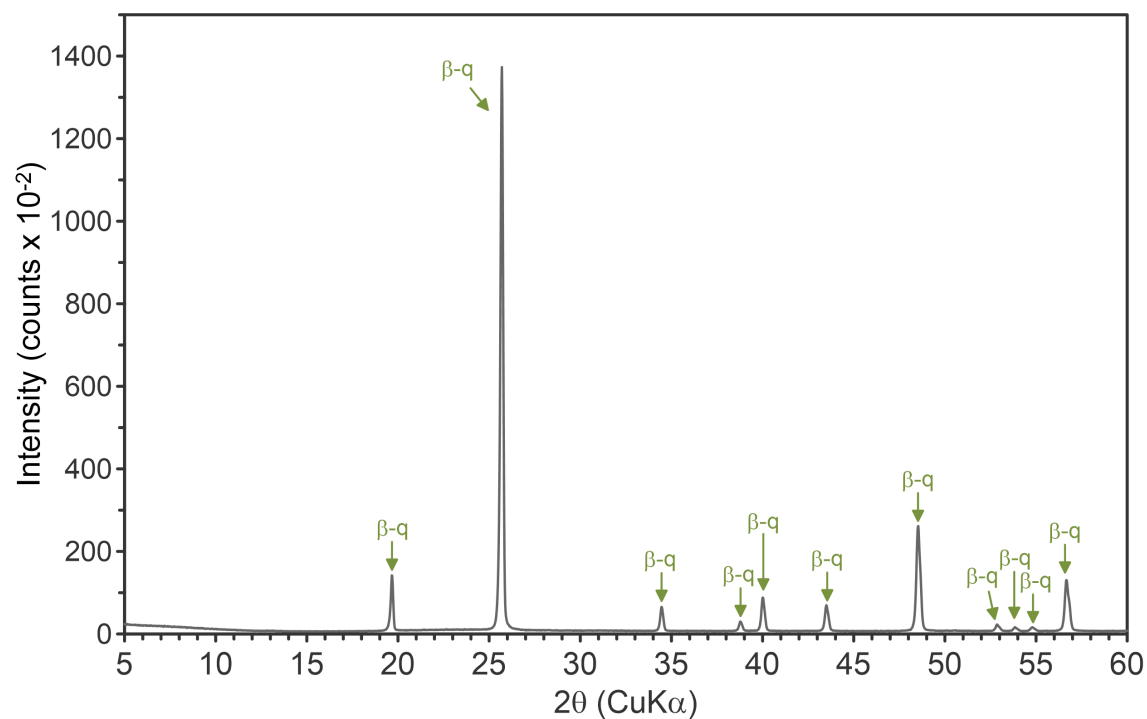


Figure S6. Extended range powder-XRD pattern corresponding to Figure 9a. β -s: β -spodumene; β -q: β -quartz.

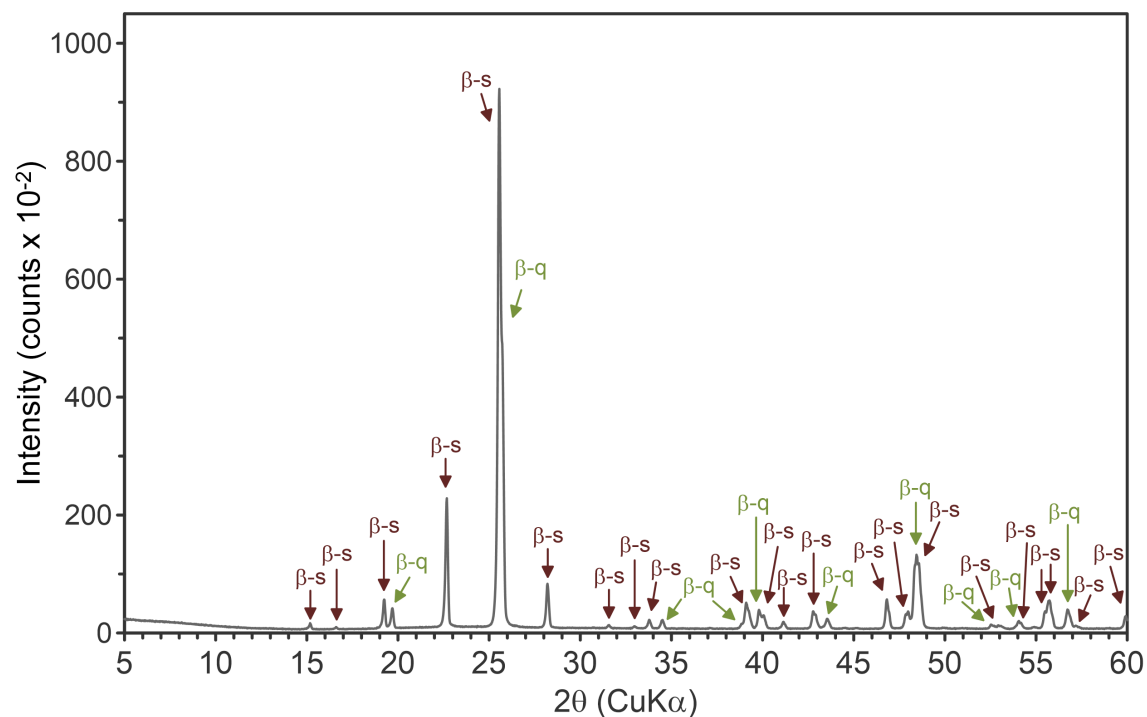


Figure S7. Extended range powder-XRD pattern corresponding to Figure 10a. β -s: β -spodumene; β -q: β -quartz.

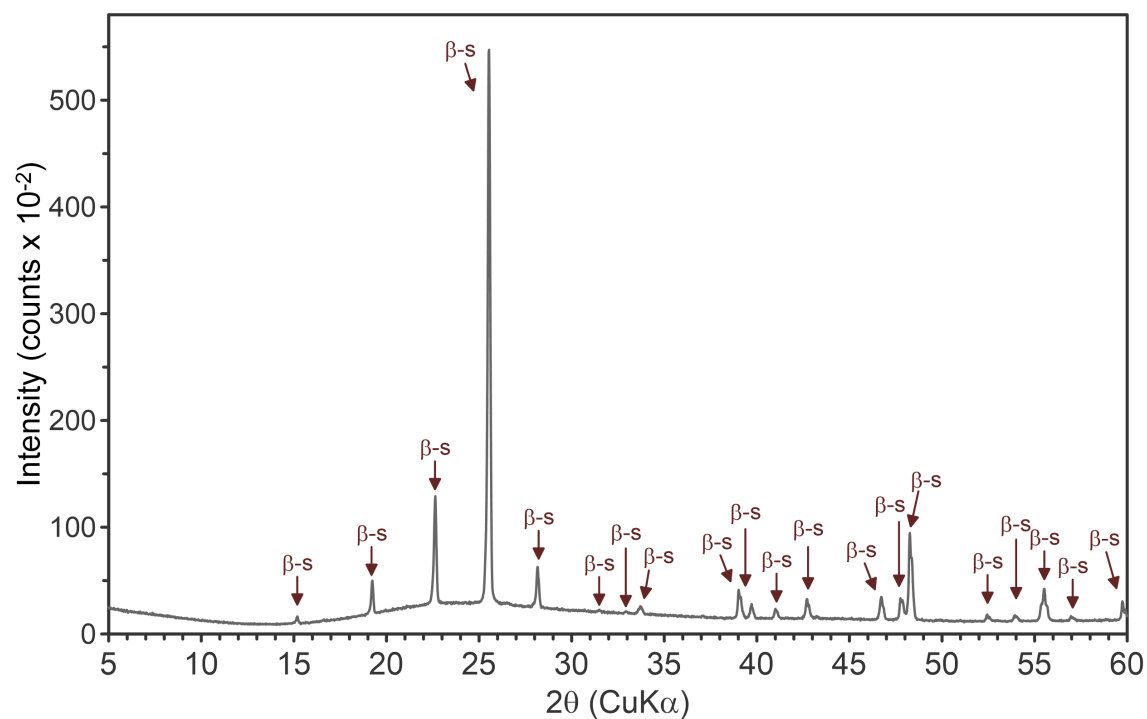


Figure S8. Extended range powder-XRD pattern corresponding to Figure 11a. β -s: β -spodumene; β -q: β -quartz.

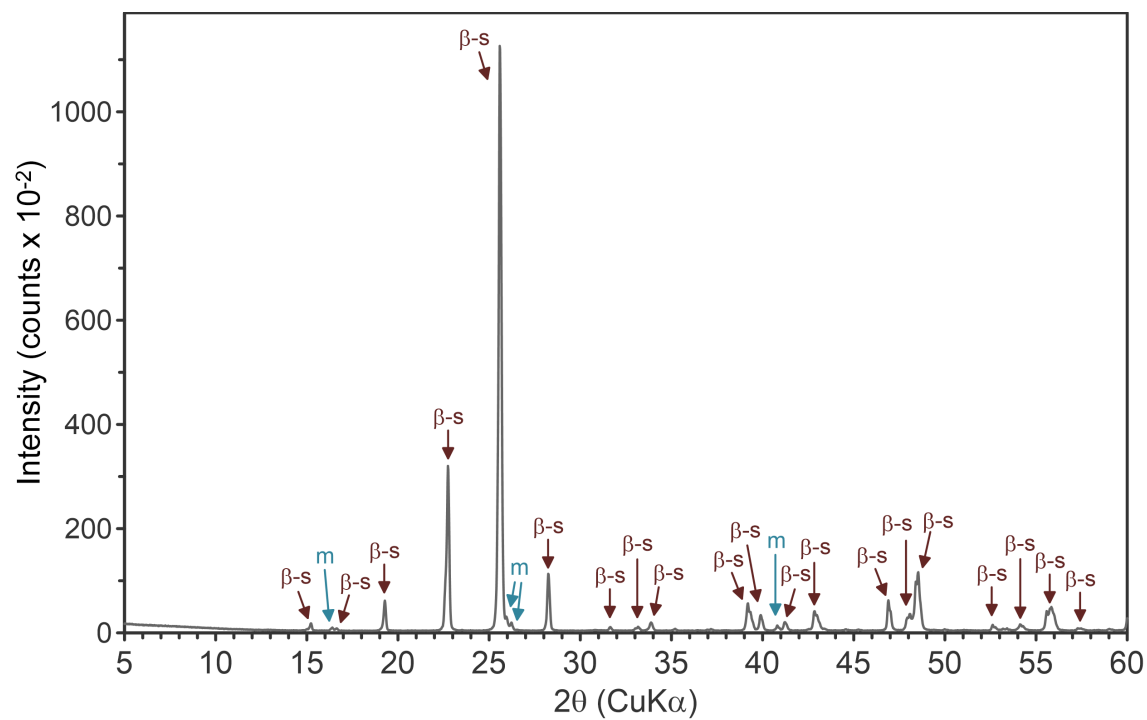


Figure S9. Extended range powder-XRD pattern corresponding to Figure 12a. β -s: β -spodumene; β -q: β -quartz; m: mullite.

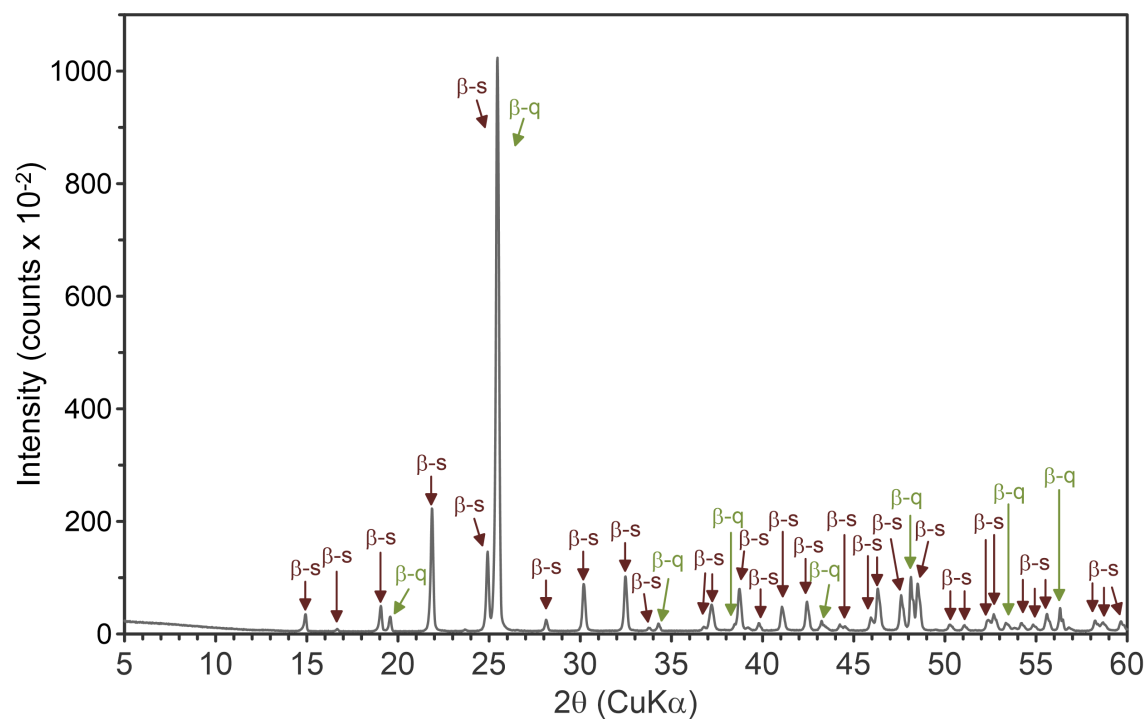


Figure S10. Extended range powder-XRD pattern corresponding to Figure 13a. $\beta\text{-s}$: β -spodumene; $\beta\text{-q}$: β -quartz.

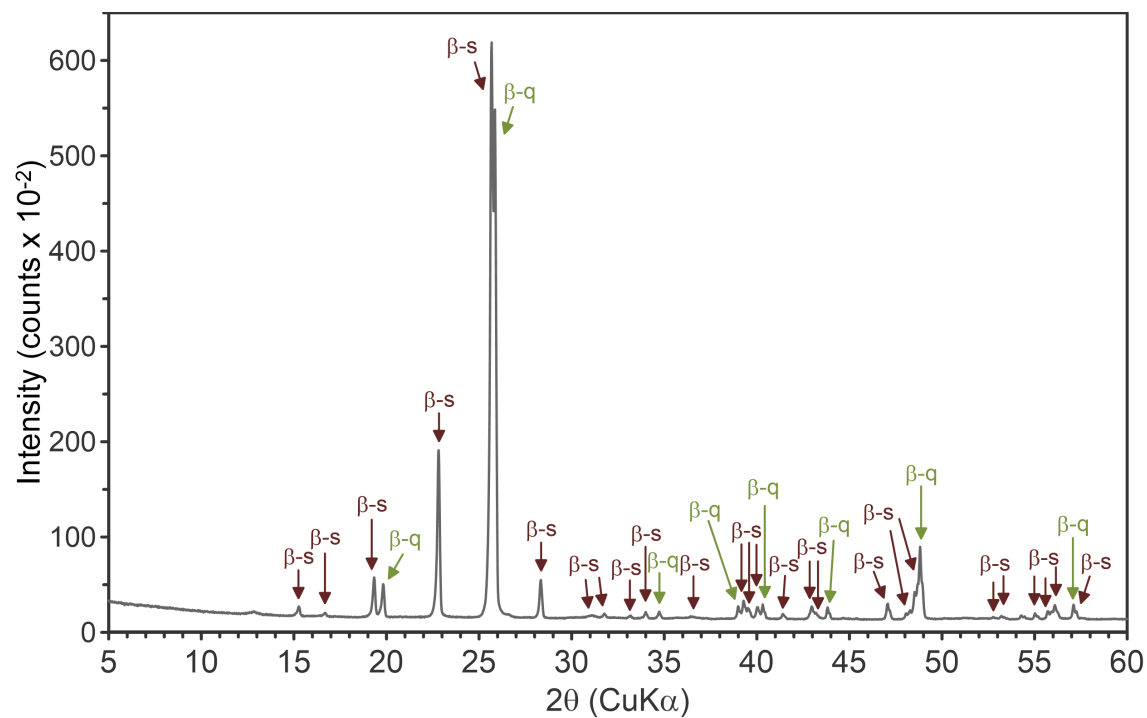


Figure S11. Extended range powder-XRD pattern corresponding to Figure 14a. $\beta\text{-s}$: β -spodumene; $\beta\text{-q}$: β -quartz.

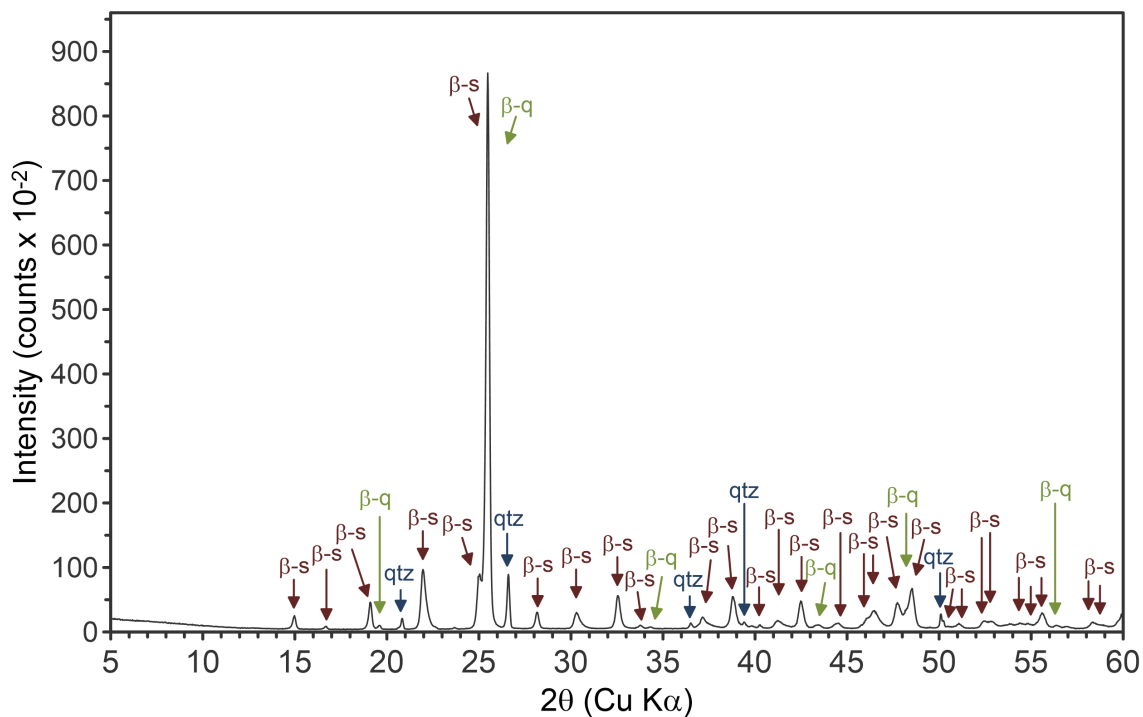


Figure S12. Extended range powder-XRD pattern collected on the decrepitated spodumene concentrate after exchange in molten NaNO_3 corresponding to Figure 15a. β -s: β -spodumene; β -q: β -quartz, qtz: quartz.

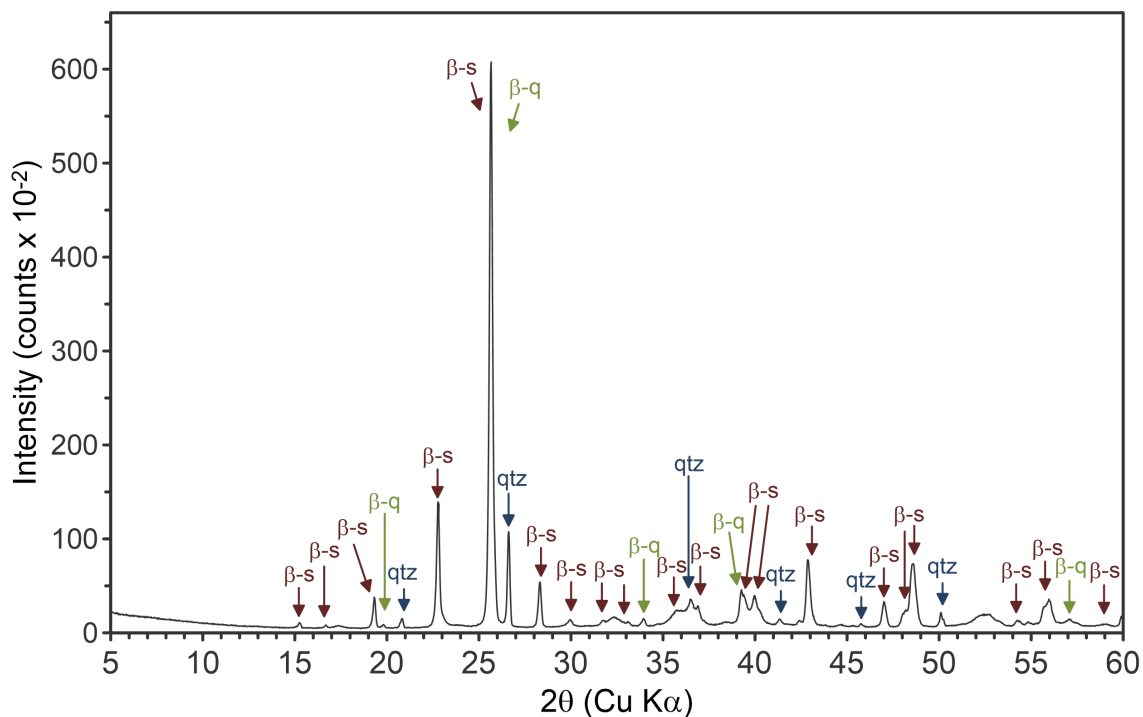


Figure S13. Extended range powder-XRD pattern collected on the decrepitated spodumene concentrate after exchange in molten $0.6 \text{ MgCl}_2 / 0.4 \text{ KCl}$ corresponding to Figure 15b. β -s: β -spodumene; β -q: β -quartz, qtz: quartz.

Rietveld analysis

Rietveld analysis of the XRD patterns obtained from the product of the solid state crystallization experiment performed using the $\text{NaAlSi}_2\text{O}_6$ glass and β -spodumene_{ss} endmembers (Section 3.1.1, Figure 8a, S5) and of the NaNO_3 molten salt exchange experiment performed on synthetic fragments with coexisting crystals of β -spodumene_{ss} and β -quartz_{ss} (Section 3.3, Figure 13a, S10). The refinement was conducted using JADE version 9 with initial structural parameters of β -spodumene_{ss} (tetragonal $P4_32_12$ [1]), β -quartz_{ss} (hexagonal $P6_222$ [2]), Na-keatite (tetragonal $P4_32_12$ [3]), and nepheline (hexagonal $P6_3$ [4]). As the main objective was to evaluate the impact of sodium for lithium substitution in β -spodumene on the unit cell dimensions, the Na/Li ratio was refined by fixing the total alkali site occupancy factor to 0.5 (e.g. Li and Peacor [1]) and linking the sodium content to that of lithium ($0.5 - \text{Li}$). The atomic coordinates of all sites were left unconstrained, however, the $[\text{Si}:\text{Al}]_{\text{atomic}}$ ratio in the appropriate sites was kept constant according to the $(\text{Li},\text{Na})\text{AlSi}_2\text{O}_6$ stoichiometry ($\text{Si}_{1.667}\text{Al}_{0.333}$). The contribution of glass (amorphous component) in the XRD pattern obtained from the product of the solid state crystallization experiment was accounted for using a pseudo-Voigt profile.

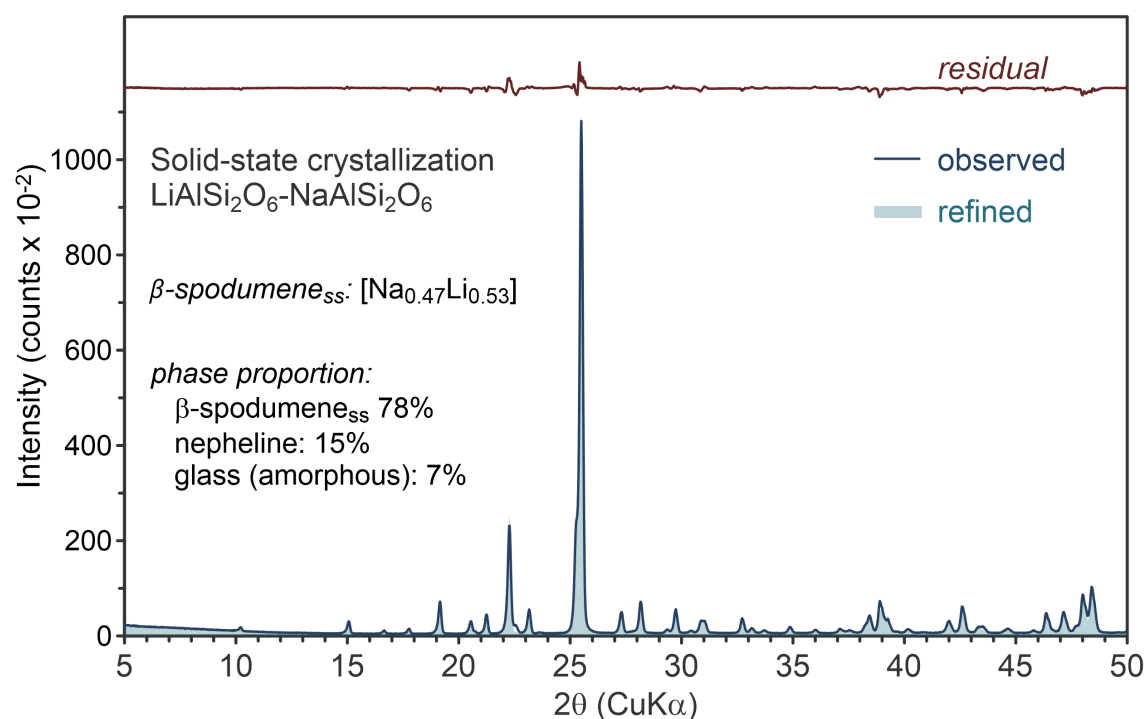


Figure S14. Observed and calculated XRD patterns from the product of the solid state crystallization experiment performed using the $\text{NaAlSi}_2\text{O}_6$ glass and β -spodumene_{ss} endmembers. The residual pattern is plotted at the same intensity scale but offset for clarity. Also shown are the calculated relative proportion of Na and Li in β -spodumene_{ss} as well as the phase proportion derived from the Rietveld refinement.

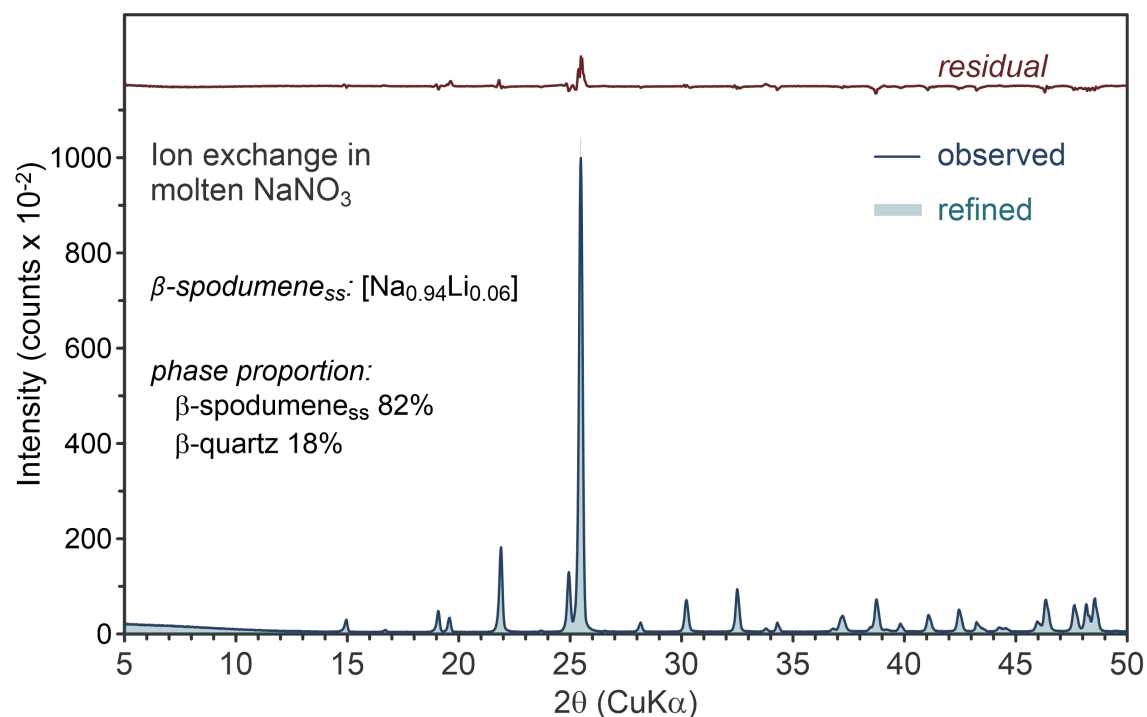


Figure S15. Observed and calculated XRD patterns from the product of the NaNO_3 molten salt exchange experiment performed on synthetic fragments with coexisting crystals of β -spodumene_{ss} and β -quartz_{ss}. The residual pattern is plotted at the same intensity scale but offset for clarity. Also shown are the calculated relative proportion of Na and Li in β -spodumene_{ss} as well as the phase proportion derived from the Rietveld refinement.

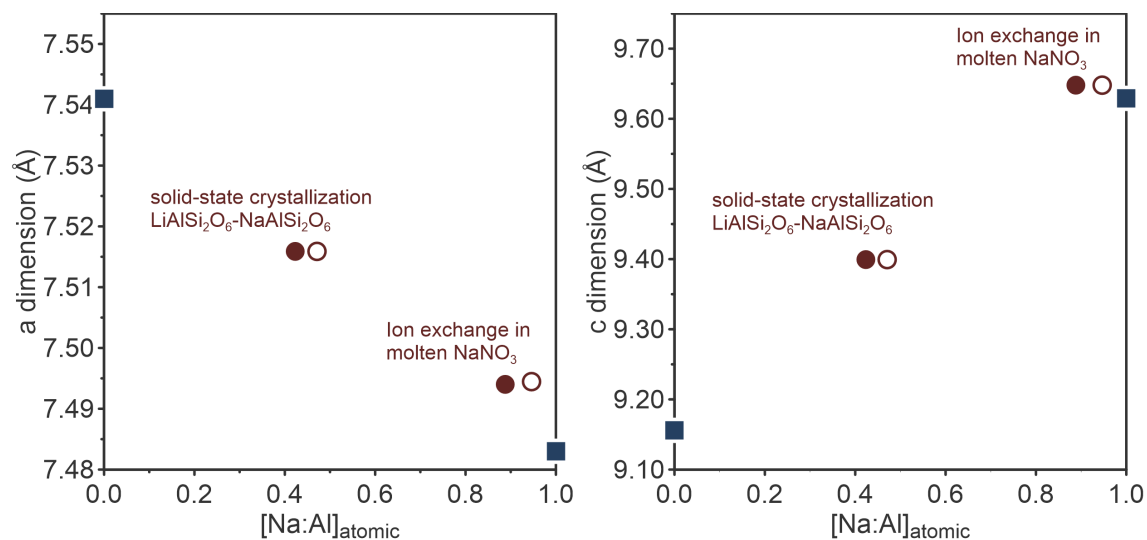


Figure S16. Variation of the a and c unit cell dimensions of β -spodumene_{ss} as a function of the $[\text{Na}:\text{Al}]_{\text{atomic}}$ ratio as measured by EPMA (filled circles) and calculated by Rietveld refinement (empty circles). The blue squares correspond to the cell dimensions values for the $\text{LiAlSi}_2\text{O}_6$ and $\text{NaAlSi}_2\text{O}_6$ endmembers from Li and Peacor [1] and Baumgartner and Müller [3], respectively.

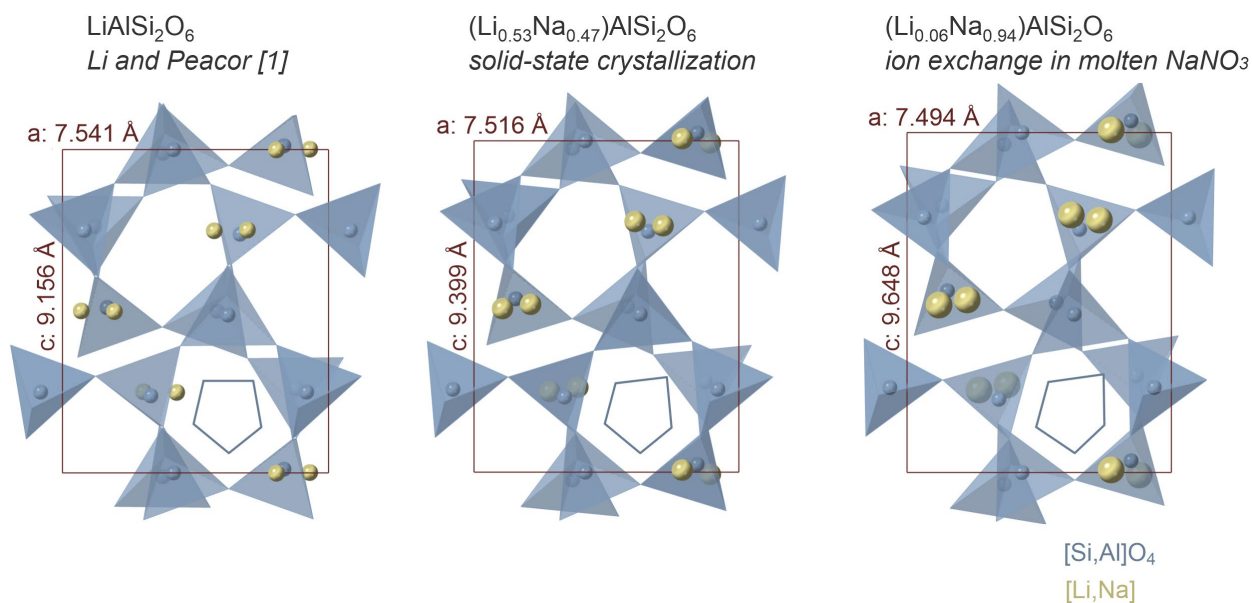


Figure S17. β -spodumene_{ss} model structures (constructed with CrystalMaker X) projected along the [100] direction for the $\text{LiAlSi}_2\text{O}_6$ endmember (crystal data from Li and Peacor [1]) and those resulting from the Rietveld refinement of the XRD patterns shown in Figure S14 and S15. The small drawn pentagons emphasize the progressive deformation of the tetrahedral framework ($[\text{Si,Al}]\text{O}_4$), resulting in an expansion along the c axis and a slight contraction along the a direction. As Li and Na are considered disordered, the alkali cation (yellow) is displayed with an effective size corresponding to the average of the ionic radii of Li and Na in fourfold coordination [5] weighted by their calculated relative concentrations in the alkali site.

References

- [1] Li, C.-T.; Peacor, D.R. The crystal structure of $\text{LiAlSi}_2\text{O}_6$ II (“ β -spodumene”). *Z. Kristallogr.* 1968, 126, 46–65. <https://doi.org/10.1524/zkri.1968.126.16.46>
- [2] Li, C.-T. The crystal structure of $\text{LiAlSi}_2\text{O}_6$ III (high quartz solid solution). *Z. Kristallogr.* 1968, 127, 327–348. <https://doi.org/10.1524/zkri.1968.127.5-6.327>
- [3] Baumgartner, B.; Müller, G. Framework distortion by large ions in $\text{MAI}_2\text{Si}_2\text{O}_6$ aluminosilicates with keatite structure. *Eur. J. Mineral.* 1990, 2, 155–162. <https://doi.org/10.1127/ejm/2/2/0155>.
- [4] Kumar, A.; Dhoble, S.J.; Peshwe, D.R.; Bhatt, J. Structural and photoluminescence properties of nepheline-structure $\text{NaAlSi}_3\text{O}_8:\text{Dy}^{3+}$ nanophosphors. *J. Alloys Compd.* 2014, 609, 100–106. <https://doi.org/10.1016/j.jallcom.2014.04.153>
- [5] Shannon, R.D. Revised effective ionic radii and systematic studies of interatomic distances in halides and chalcogenides. *Acta Crystallogr.* 1976, A32, 751–767. <https://doi.org/10.1107/S0567739476001551>